*Acta Cryst.* (1985). A41, 591-597

# Dynamical Effects in X-ray–Thermal Phonon Interactions in Symmetric Bragg Reflections*

BY F. WASSERSTEIN-ROBBINS† AND H. J. JURETSCHKE

*Polytechnic Institute of New York, 333 Jay Street, Brooklyn, New York 11201, USA*

(*Received* 31 *August* 1984; *accepted* 10 *July* 1985)

## Abstract

The selfconsistent theory of X-ray–phonon coupling near a symmetric two-beam Bragg reflection is developed for single-phonon transitions, in the dynamical angular region where both the initial and final states may be two-beam modes. Explicit results are obtained for an incident-beam direction close to but not at the Bragg angle. Selection rules for transitions between various branches of the dispersion surfaces, based on boundary conditions for internally excited modes, and influenced by primary extinction, lead to the kinematically expected maximum in TDS on the opposite side of the Bragg angle as the specularly reflected beam, but also introduce additional dynamical effects that, in particular, suppress phonon coupling into the angular region of total reflection. The results are compared with earlier theories, and with two experiments using very small angular offsets from the Bragg angle for the incident beam. They offer a detailed interpretation for defect lines observed in TDS when this angular offset is large enough so that the incident beam produces no comparable elastic scattering into the region of total reflection.

## 1. Introduction

The first-order interaction of X-rays with thermal phonons leads to the well known thermal diffuse scattering (TDS) accompanying X-ray diffraction. TDS peaks in intensity whenever the scattering vector

$$\mathbf{Q} = \mathbf{K}_f - \mathbf{K}_0 \tag{1}$$

connecting the incident wave vector $\mathbf{K}_0$ and the scattered wave vector $\mathbf{K}_f$ is in the neighborhood of a reciprocal-lattice vector $\mathbf{H}$. For low-energy phonons of wave vector $\mathbf{q}$, $\mathbf{K}_0$ and $\mathbf{K}_f$ belong to X-rays of essentially the same energy, and conservation of momentum requires

$$\mathbf{Q} = \mathbf{H} + \mathbf{q}. \tag{2}$$

At normal temperatures, the scattering for given $\mathbf{Q}$ into an element $dq_x\, dq_y\, dq_z$ is proportional to (*e.g.* Willis & Pryor, 1975)

$$|\mathbf{Q}|^2 |F_Q|^2 (k_B T/q^2)\langle g^2/v_p^2\rangle, \tag{3}$$

where $v_p$ is a phonon velocity and $\langle g^2/v_p^2\rangle$ is the contribution of $1/v_p^2$ from the three acoustic branches weighted according to the projection $g$ of their mode amplitudes along $\mathbf{Q}$. The structure factor $F$ includes a Debye–Waller factor appropriate to $\mathbf{Q}$. For very small $\mathbf{q}$, $\mathbf{Q} \simeq \mathbf{H}$, and (3) exhibits the conventional divergence of TDS as $q$ goes to zero.

In a symmetric two-beam Bragg configuration, however, where one samples the output at different angles $\theta_{\text{out}}$ for a fixed angle of incidence $\theta_{\text{in}}$ away from the Bragg angle (here we measure all angles relative to the Bragg angle $\theta_B$), the observed TDS output has a different $q$ dependence. $q$ never goes to zero, but instead reaches a minimum, which, according to kinematic theory (*e.g.* Eisenberger, Alexandropoulos & Platzman, 1972), occurs when

$$\theta_{\text{out}} = -\theta_{\text{in}} \cos 2\theta_B. \tag{4}$$

In addition, since in such an experiment the detector usually covers a wide angular range of exit angles in the direction normal to the plane of incidence, a given $\theta_{\text{out}}$ samples all phonons with arbitrary components of $\mathbf{q}$ normal to this plane (Iida & Kohra, 1979). Hence, instead of (3), the observed TDS should show a $1/q_0$ dependence, where $q_0$ is the common component in the plane of incidence of all contributing $\mathbf{q}$. This dependence is shown in Fig. 1 as a function of $\theta_{\text{out}}$ for two values of $\theta_{\text{in}}$, for the 220 reflection of Ge, based on the expression

$$q_0^2 = k^2(\theta_{\text{out}}^2 + \theta_{\text{in}}^2 + 2\cos 2\theta_B \theta_{\text{out}} \theta_{\text{in}}), \tag{5}$$

where $k = 2\pi/\lambda$. The $\theta$'s in (5) and in the theory below are measured in radians, but in all graphs, especially those relating to experiments, the corresponding $\theta$ is conveniently expressed in seconds of arc (s or ″). Equation (5) follows from the conservation requirement that $q_0$ must connect two points on the kinematic dispersion surfaces at constant energy, in the plane of incidence, as shown in Fig. 2(*a*).

The angles $\theta$ in Fig. 1 were chosen for comparison with the experimental data of Eisenberger *et al.* (1972), from now on designated as EAP, who attempted to apply the above $\theta_{\text{in}}$-offset method to study very-long-wavelength phonons. With a

* Supported in part by the Joint Services Electronics Program Contract No. F49620-82-C-0084.

† Present address: Department of Mathematics, College of Staten Island, Staten Island, New York 10301, USA.

0108-7673/85/060591-07$01.50 

grooved-crystal collimator for restricting the divergence of the incident beam, they were able to identify the maxima of Fig. 1 as roughly obeying (4) in the range $10 < \theta_{in} < 1000''$. They also saw additional details in the diffracted structure that have not been examined theoretically. This paper offers, among other results, such an analysis, in the process concluding that their results are, in fact, unlikely to have been caused by TDS. A similar technique deliberately aimed at studying other causes of diffuse scattering has recently been developed by Afanas'ev and coworkers (Afanas'ev, Koval'chuk, Lobanovich, Imamov, Aleksandrov & Melkonyan, 1981).

A proper theory of X-rays interacting with phonons whose $q$ is comparable to the width of the range of total reflection of a Bragg peak must include dynamical effects. Such effects come into play in a number of ways. An obvious source arises from the shape of the dynamical dispersion surfaces. As shown in Fig. 2(*b*), the real part of these dispersion surfaces is strongly perturbed in the region of total reflection. Hence the value of $q_0$ connecting a given set of angles $(\theta_{in}, \theta_{out})$ is altered when either of these angles is close to zero. In addition, the same dynamic effects that cause asymmetries in the specularly (elastic) reflected intensity in this region can be expected also to introduce asymmetries in the X-ray-phonon coupling. Furthermore, since the final X-ray state, and perhaps also the initial state, is a two-field state when close to the region of total reflection, appropriate boundary conditions have to be observed to ensure that the emerging field created by phonon coupling arises entirely from an internal source. Finally, among other questions that have to be resolved by a consistent theory is that it is not obvious how, in a dynamical scheme, the phonons connect states lying on the normal sheet of the dispersion surface with states lying on the anomalous one, as implied in Fig. 2(*b*).

We expect that most dynamical contributions will alter (3) primarily through a factor $f$ that measures the effective relative strength of the X-ray–phonon interaction. Hence, the dynamical equivalent of (3) – after integrating over all phonon components $q_y$ perpendicular to the plane of incidence – gives the TDS into $dq_x\, dq_z$ as proportional to

$$H^2|F_H|^2 k_B T(f/q_0)\langle g^2/v_p^2\rangle. \qquad (6)$$

As already mentioned, (6) differs from (3) not only because of the factor $f$, but also because $q_0$ connecting a given pair $(\theta_{in}, \theta_{out})$ is no longer given by (5), but must be obtained from the actual dispersion surface, such as in Fig. 2(*b*).

The present work builds on earlier discussions of some of these questions (*e.g.* Kainuma 1961; O'Connor, 1967; Afanas'ev & Kagan, 1967; Afanas'ev, Kagan & Chukovskii, 1968; Köhler, Möhling & Peibst, 1974), especially by including consistent boundary conditions for phonon-excited modes in a systematic treatment based on phonon-coupled X-ray modes tied to many-sheeted dynamical dispersion surfaces. This characterization becomes particularly important in the immediate neighborhood of the totally reflecting region. Since the distortions of an ideal crystal by thermal phonons are small, the more general treatment of scattering in distorted crystals by Kuriyama (1972) is not needed here.

In the following section, we will determine $f$ and $f/q_0$ for the case when $\theta_{in}$ is large compared to the angular width of the Bragg reflection, but for arbitrary values of $\theta_{out}$, and indicate the relation of our results to the earlier treatments. § 3 compares the theory to the EAP and other experiments, and the final section

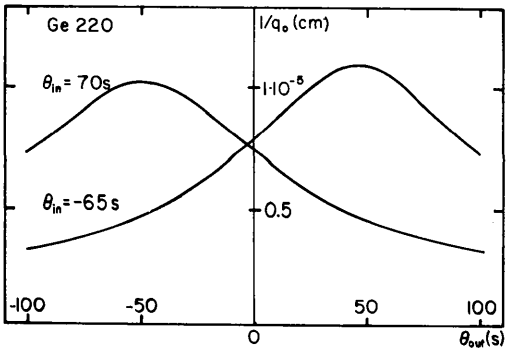


Fig. 1. Kinematic prediction of the $1/q_0$ dependence of the TDS intensity *vs* exit angle $\theta_{out}$, for two fixed angles of incidence $\theta_{in}$ of the symmetric Ge 220 Bragg reflection. All angles are relative to the Bragg angle $\theta_B$. The curves go into their mirror images relative to the vertical axis with sign reversal of $\theta_{in}$.

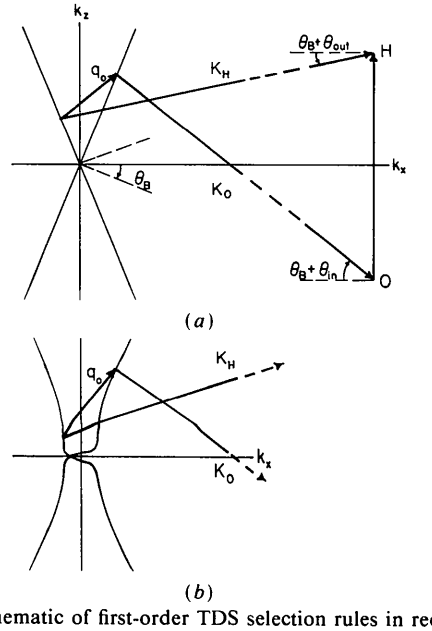


Fig. 2. Schematic of first-order TDS selection rules in reciprocal space connecting $\mathbf{q}_0$, $\mathbf{K}_0$, $\mathbf{K}_H$ and $\mathbf{H}$, (*a*) with respect to the kinematic dispersion surfaces of the $0H$ reflection, relative to the Lorentz point; (*b*) with respect ot the corresponding dynamical dispersion surfaces. $\mathbf{q}_0$ is chosen to connect the same $\theta_{in} > 0$ and $\theta_{out} < 0$ as in (*a*).

discusses additional applications of our results. A preliminary account of this work was presented at the January 1983 meeting of the American Physical Society (Wasserstein-Robbins & Juretschke, 1983).

## 2. Theory

Our starting point is the symmetric two-beam Bragg reflection. In terms of the notation of Batterman & Cole (1964), it is described, for $\sigma$ polarization, by two scalar equations for the transverse incident and reflected field amplitudes $E_0$, $E_H$:

$$\begin{aligned} 2\xi_0 E_0 + k\Gamma F_{\bar{H}} E_H &= 0 \\ k\Gamma F_H E_0 + 2\xi_H E_H &= 0, \end{aligned} \tag{7}$$

where $\xi_0$ and $\xi_H$ are the complex changes in magnitude of $\mathbf{K}_0$ and $\mathbf{K}_H$ from their average value within the crystal:

$$\xi_i = (\mathbf{K}_i \,.\, \mathbf{K}_i)^{1/2} - k(1 - \tfrac{1}{2}\Gamma F_0) \tag{8}$$

and $\Gamma = e^2/(\varepsilon_0 m\omega^2 v_{\text{cell}})$. $\xi_0$ and $\xi_H$ are related, at a given angle of incidence $\theta_{\text{in}}$ ($= \theta_{\text{out}}$), by

$$\xi_0 + \xi_H = \delta = k(i\Gamma F_0'' - \theta_{\text{in}} \sin 2\theta_B). \tag{9}$$

If the effect of phonons is described by rigid atomic displacements of the form

$$\mathbf{U}(r) = \sum_{j=1}^{N} \mathbf{u}_j \sin(\mathbf{q}_j \,.\, \mathbf{r} - \omega_j t + \varphi_j), \tag{10}$$

the generalization of (7) that includes all exchanges of a single $\mathbf{q}$ is (*e.g.* O'Connor, 1967; Afanas'ev *et al.*, 1968; Köhler *et al.*, 1974; Wasserstein-Robbins, 1982)

$$\begin{aligned} &2\xi_{00}E_{00} + F_{0\bar{H}}E_{0H} \\ &\quad = \sum_{j=1}^{N} (e^{-i\varphi_j} F_{j\bar{H}} E_{jH} - e^{i\varphi_j} F_{j\bar{H}} E_{\bar{j}H}) \\ &F_{0H}E_{00} + 2\xi_{0H}E_{0H} \\ &\quad = -\sum_{j=1}^{N} (e^{-i\varphi_j} F_{jH} E_{j0} - e^{i\varphi_j} F_{jH} E_{\bar{j}0}) \\ &2\xi_{j0}E_{j0} + F_{0\bar{H}}E_{jH} = -e^{i\varphi_j} F_{j\bar{H}} E_{0H} \\ &F_{0H}E_{j0} + 2\xi_{jH}E_{jH} = e^{i\varphi_j} F_{jH} E_{00} \\ &2\xi_{\bar{j}0}E_{\bar{j}0} + F_{0\bar{H}}E_{\bar{j}H} = e^{-i\varphi_j} F_{j\bar{H}} E_{0H} \\ &F_{0H}E_{\bar{j}0} + 2\xi_{\bar{j}H}E_{\bar{j}H} = -e^{-i\varphi_j} F_{jH} E_{00}, \end{aligned} \tag{11}$$

$j = 1, \ldots, N$, where $j$ and $\bar{j}$ refer to the absorption of $\mathbf{q}_j$ and its emission $-\mathbf{q}_j$, respectively. The set $(\xi_{00}, \xi_{0H})$ belongs to the central beam existing even in the absence of phonons and, because of momentum conservation, the other sets $(\xi_{j0}, \xi_{jH})$ are related to it by

$$\xi_{j0} = \xi_{00} + \Delta_{j0}, \qquad \xi_{jH} = \xi_{0H} + \Delta_{jH} \tag{12}$$

with

$$\Delta_{j0} = (\mathbf{q}_j \,.\, \mathbf{K}_0)/k, \qquad \Delta_{jH} = (\mathbf{q}_j \,.\, \mathbf{K}_H)/k. \tag{13}$$

To the lowest orders of interaction, the reduced structure factors in (11) are given by

$$\begin{aligned} F_{0H} &= k\Gamma F_H \prod_{m=1}^{N} J_0(\mathbf{H} \,.\, \mathbf{u}_m), \\ F_{jH} &= k\Gamma F_H J_1(\mathbf{H} \,.\, \mathbf{u}_j), \end{aligned} \tag{14}$$

with $J_0$ and $J_1$ ordinary Bessel functions, so that $F_{0H}$ includes a Debye–Waller-factor correction. Equations (11) differ from those given by O'Connor (1967) in that the Debye–Waller factor attached to $F_{0H}$ in (14) is a natural consequence of including back-coupling into the central beam, so that this factor need not be introduced separately (see also Köhler *et al.*, 1974). In addition, (11) assumes that $H \gg q$, so that all terms proportional to $J_1(\mathbf{q} \,.\, \mathbf{u})$ are omitted, and $(\mathbf{H}+\mathbf{q}) \,.\, \mathbf{u}$ is approximated by its main term.

When all $F_{jH} = 0$, (11) represents $2N+1$ independent symmetric two-beam cases, differing, at a given $\delta$, by the various angles of incidence defined by their respective $\mathbf{q}_j$. If only the central beam couples to an externally incident field, none of the other modes are excited.

In the presence of coupling terms on the right side, each mode in (11) is described by $2N+1$ field pairs (Wasserstein-Robbins, 1982). For example, the $m$th mode consists of the set

$$\begin{aligned} &E_{00}(m), E_{0H}(m); \ldots; E_{j0}(m), \\ &E_{jH}(m); \ldots; E_{\bar{j}0}(m), E_{\bar{j}H}(m); \ldots. \end{aligned}$$

However, the structure of (11) shows that all fields for $j \neq 0$ couple to each other only through the central beam. To lowest order, therefore, we can neglect this interaction, so that only the mode attached to the central beam, $m = 0$, retains its full complement of fields

$$\begin{aligned} &E_{00}(0), E_{0H}(0); \ldots; E_{j0}(0), \\ &E_{jH}(0); \ldots; E_{\bar{j}0}(0), E_{\bar{j}H}(0); \ldots, \end{aligned}$$

while all other modes reduce back to two-beam cases $j = m$, such as $[E_{j0}(j), E_{jH}(j)]$. Hence, all phonons can be treated independently and their contributions are additive. For the $j$th phonon, the reflected field $E_{jH}$ is therefore given by the sum of only two terms

$$E_{jH} = E_{jH}(0) + E_{jH}(j), \tag{15}$$

subject to the condition that there is no net incident field associated with this phonon-excited reflected field:

$$E_{j0} = 0 = E_{j0}(0) + E_{j0}(j). \tag{16}$$

The four field amplitudes appearing in (15) and (16) can be related to $E_{00}$ through (11), and lead to the

expression for the reflected field

$$\frac{E_{jH}}{E_{00}} = \frac{2e^{i\varphi_j}F_{jH}\xi_{00}(0)}{F_{0H}F_{0\bar{H}}} \times \left[\frac{\xi_{0H}(0)\Delta_{j0}+\xi_{j0}(j)\Delta_{jH}}{\Delta_{j0}\Delta_{jH}+\xi_{00}(0)\Delta_{jH}+\xi_{0H}(0)\Delta_{j0}}\right]. \quad (17)$$

A similar expression holds for $E_{\bar{j}H}/E_{00}$.

Here $\xi_{00}(0)$ and $\xi_{0H}(0)$ refer to the normal branch of the central beam and $\xi_{j0}(j)$ belongs to the normal branch of the independent two-beam solution corresponding to an incident angle $\theta_{in}(j)$ defined, in analogy to (9), by

$$\xi_{j0}(j)+\xi_{jH}(j) = \delta+\Delta_{j0}+\Delta_{jH} = k[i\Gamma F_0'' - \theta_{in}(j)\sin 2\theta_B]. \quad (18)$$

Through a series of geometrical relations involving (12) and (18), (17) can be simplified to the form

$$\frac{E_{jH}}{E_{00}} = -\frac{2e^{i\varphi_j}F_{jH}\xi_{00}(0)}{F_{0H}F_{0\bar{H}}}\left[\frac{\xi_{0H}(0)-\xi_{j0}(j)}{\Delta_{j0}-\xi_{jH}(j)+\xi_{00}(0)}\right], \quad (19)$$

leading to a scattered intensity

$$\left|\frac{E_{jH}}{E_{00}}\right|^2 = \frac{|F_{jH}F_{j\bar{H}}|}{4|\xi_{0H}(0)|^2} \times \frac{[\xi_{0H}'(0)-\xi_{j0}'(j)]^2+[\xi_{0H}''(0)-\xi_{j0}''(j)]^2}{[\Delta_{j0}-\xi_{jH}'(j)+\xi_{00}'(0)]^2+[\xi_{00}''(0)-\xi_{jH}''(j)]^2} \quad (20)$$

with primes and double primes designating real and imaginary parts.

Through (9) the incident angle $\theta_{in}$ is fixed by $[\xi_{00}(0), \xi_{0H}(0)]$. Similarly, through (18) the exit angle $\theta_{out}(j)$ $[=\theta_{in}(j)]$ is defined by the set $[\xi_{j0}(j), \xi_{jH}(j)]$. Hence, (20) provides the scattered intensity due to the $j$th phonon into its $\theta_{out}$, for given $\theta_{in}$. To find the total intensity into a given $\theta_{out}$, we must sum (20) over all phonons connecting $\theta_{in}$ to this one output angle.

In carrying out this sum, we make use of two convenient aspects of the structure of (20). Firstly, since for thermal phonons all the dispersion surfaces of interest are independent of $k_y$, the direction normal to the plane of incidence, we need consider explicitly only $\mathbf{q}_j$'s in the $k_x - k_z$ plane of incidence. The sum over the third component, $q_y$, has no dynamical aspects, but, as mentioned in § 1, depends only on the phonon distribution. Secondly, since for fixed $\theta_{in}$ and $\theta_{out}$ all the $\xi$'s in (20) are constant, (20) is only a function of the variable $\Delta_{j0}$ [related to $\mathbf{q}_j$ through (13)], which appears explicitly as well as in $|F_{jH}F_{j\bar{H}}|$.

As shown in Fig. 3($a$), the sum involves all $\mathbf{q}_j$'s originating along the dashed vertical line $V$, and not necessarily only those connecting the dispersion surfaces $0H$ and 00. However, the sum is dominated by those terms of (20) for which

$$\Delta_{j0} \simeq \xi_{jH}'(j) - \xi_{00}'(0), \quad (21)$$

as long as $\xi_{0H}'(0) \gg \xi_{j0}'(j)$, which is everywhere except when a phonon connects two points within the totally reflecting region, *i.e.* when both $\theta_{in}$ and $\theta_{out}$ are small. Hence, as a function of $\Delta_{j0}$, (20) is a Lorentzian sharply peaked at the value given by (21). If $|F_{jH}F_{j\bar{H}}|$ is a slowly varying function of $\Delta_{j0}$, the integral is easily carried out:

$$\int_{-\infty}^{\infty} |E_{jH}/E_{00}|^2 \, dq_z = \int_{-\infty}^{\infty} |E_{jH}/E_{00}|^2 (\partial q_z/\partial\Delta_0)_{q_x} \, d\Delta_0 = \frac{\pi|F_{jH}F_{j\bar{H}}|}{\sin\theta_B} \frac{[\xi_{0H}'(0)-\xi_{j0}'(j)]^2+[\xi_{0H}''(0)-\xi_{j0}''(j)]^2}{|\xi_{0H}(0)|^2|\xi_{00}''(0)-\xi_{jH}''(j)|}, \quad (22)$$

where $|F_{jH}F_{j\bar{H}}|$ is evaluated for the dominant phonon $\mathbf{q}_j$ satisfying (21). Geometrically, the condition (21) corresponds to the intersection of the dashed vertical line $V$ defining $\theta_{out}$ in Fig. 3($a$) with the $0H$ sheet, *i.e.* the anomalous sheet of the standard dispersion surface. Therefore the construction first indicated in Fig. 2($b$), based on kinematic momentum conservation, is now formally justified. Under the conditions specified above with respect to (21), no significant contribution to the scattered intensity comes from the other intersection where the vertical $V$ crosses the 00 sheet, even though momentum conservation using independent two-beam states is equally satisfied there. This indicates that within the approximations inherent in our treatment any phonon coupling must always involve a Bragg reflection. Equation (22) differs from the expression derived by O'Connor (1967) for the Bragg case because of boundary conditions other than the dynamical ones of (15) and (16). These differences are particularly important when $\xi_{0H}(0)$ and $\xi_{j0}(j)$ are close to each other. Similarly, (22) differs from the corresponding result of Afanas'ev *et al.* (1968) where the anomalous solution of the $j$th branch was used to satisfy (16).

The fact that in Fig. 3($a$) the coupling appears to excite a state on the anomalous branch of the dispersion surface is merely a result of the compact representation of the transition in terms of the central sheets 00 and $0H$ of the full dispersion surface of $2N+1$ sheets. As shown and explained in Fig. 3($b$), in the actual state of affairs the (anomalous) $jH$ sheet perturbs the (normal) 00 sheet at their intersection, to produce a reflection into the $\mathbf{K}_H$ direction, completely analogous to a weak two-beam interaction. It is, of course, only in the representation of Fig. 3($b$) that the proper boundary conditions on the phonon-excited X-rays can be satisfied. The geometrical construction of Fig. 3($b$) also indicates that for given $\theta_{in}$

and $\theta_{out}$ a phonon $\mathbf{q}_j$ is *either* absorbed *or* emitted, but not both. Hence we are justified in treating either $E_{jH}(0)$ or $E_{\bar{j}H}(0)$ as large, but not both, in satisfying these boundary conditions.

The last factor in (22) represents the modification introduced by the dynamical treatment of X-rays. Since for $\theta_{out}$ large it approaches asymptotically the value $1/\delta''$ ($\delta'' = k\Gamma F_0''$), we can rewrite it as $f/\delta''$, with

$$f = \delta''\{[\xi'_{0H}(0) - \xi'_{j0}(j)]^2 + [\xi''_{0H}(0) - \xi''_{j0}(j)]^2\}/|\xi_{0H}(0)|^2|\xi''_{00}(0) - \xi''_{jH}(j)|. \quad (23)$$

Finally, using the first term in the series expansion of $J_1$ in (14), and the standard relation of $u_j^2$ to $kT$ (*e.g.* James, 1965), and taking into account both the absorption and emission of $\mathbf{q}_j$ and $-\mathbf{q}_j$, respectively, we obtain the full expression for the TDS intensity into a range $d\theta_{out}$ for a $\sigma$-polarized incident beam at $\theta_{in}$

$$dI(\theta_{in}, \theta_{out}) = (k^2\Gamma/32\pi\rho)H^2(|F_H|^2/F_0'')k_BT(f_\sigma/q_0) \times \langle g^2/v_p^2\rangle \, d\theta_{out}, \quad (24)$$

where $\rho$ is the mass density of the crystal, $f_\sigma$ is given by (23), and the proper expression for $q_0$ is

$$q_0^2 = (\sin^2 2\theta_B)^{-1}\{[\xi'_{jH}(j) - \xi'_{00}(0)]^2 + [\xi'_{j0}(j) - \xi'_{0H}(0)]^2 - 2\cos 2\theta_B[\xi'_{jH}(j) - \xi'_{00}(0)][\xi'_{j0}(j) - \xi'_{0H}(0)]\}. \quad (25)$$

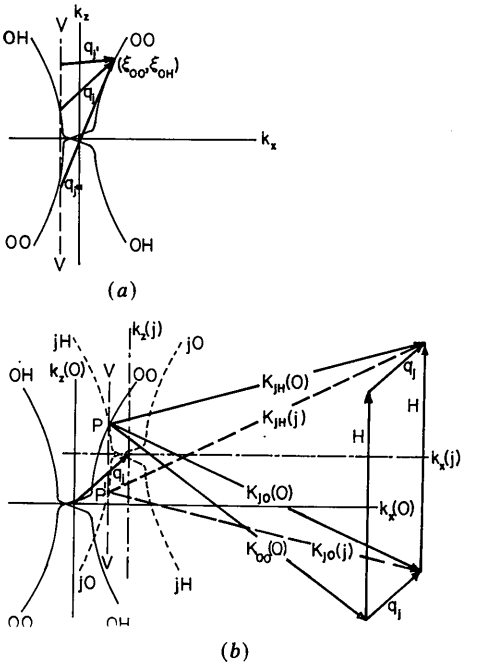


Fig. 3. Dynamical $N$-phonon coupling to X-rays, for the same $\theta_{in}$ and $\theta_{out}$ as in Fig. 2. (*a*) Single dispersion surface representation: all phonons originating on the vertical $V$ and terminating at the tiepoint ($\xi_{00}$, $\xi_{0H}$), such as $q_j$, $q_{j'}$ and $q_{j''}$, contribute to the sum in (22); (*b*) multiple dispersion surface representation for the dominant phonon $\mathbf{q}_j$ of (*a*). The common tiepoint $P$ now corresponds to both $\theta_{in}$ of the mode [$K_{00}(0)$, $K_{0H}(0)$, $K_{j0}(0)$, $K_{jH}(0)$], relative to **H**, and $\theta_{out}$, relative to **H** displaced parallel to itself by $\mathbf{q}_j$. The two-beam mode [$K_{j0}(j)$, $K_{jH}(j)$] originating at tiepoint $P'$ is needed to satisfy (15) and (16). The contribution of all phonons is obtained by sliding the ($j0$, $jH$) dispersion surface along its vertical axis.

Equations (24) and (25) are the dynamical analogues of (3) and (5), as applied to the symmetric two-beam Bragg case, and with an offset in $\theta_{in}$ outside the angular range of the main specular reflection, *i.e.* $\theta_{in} \gg \Gamma|F'_H|/\sin 2\theta_B$. The extension of these results to the other polarization mode is obvious. However, because $f/q_0$ is peculiar to each polarization, the normal averaging for an unpolarized incident beam may not always be used.

Before relating these results to the EAP and other experiments, it should be pointed out that, as expected, the dependence of (22) and (24) on $|F_{jH}|^2/F_0''$ identifies TDS as proportional to the typical integrated intensity of a weak reflection. This inverse dependence on absorption is rarely pointed out explicitly in the TDS literature (*e.g.* Schuster & Weymouth, 1971) and appears in a kinematic treatment only if explicit account is taken of the distance into the crystal within which phonon-excited X-rays are created and can escape (Schuster, 1969). It is a natural formal consequence of any dynamical treatment.

### 3. Application to an experiment

An experiment satisfying the general conditions of the above theory was carried out by EAP (1972). In particular, the angular resolutions of both the incident and reflected intensities were such as to allow one, in principle, to look at couplings of the very-long-wavelength phonons that should show strong dynamical effects.

Fig. 4 displays the variation of $f$ predicted by (23) for the Ge 220 reflection studied by EAP, for incident beams at $\theta_{in} = \pm 70''$. The most startling feature of this figure is that $f$ decreases to less than 0·1 when $\theta_{out}$ is within the angular range of the main reflection. This indicates that in this range phonon coupling is strongly suppressed. The two main physical reasons for this behavior, both contained formally in (23), are:

(*a*) If the phonon-induced X-ray mode emanates from the region of nearly total reflection, it is a two-beam mode with $E_H$ and $E_0$ fields of comparable magnitude. But, since this mode has no incident field to couple to, $E_0$ cannot exist. Hence, $E_H$ is also suppressed;

(*b*) The large primary extinction in this angular region reduces the active depth below the crystal surface within which the X-ray–phonon interaction takes place.

The dependence of the X-ray–phonon coupling on primary extinction also explains the peak in $f$ on the low-angle side of the main reflection, corresponding to a Borrmann effect, and the slow increase in $f$ from its minimum on the high-angle side with its dispersion sheet of larger than average absorption. Finally, the increase in $f$ for $\theta_{in} < 0$ relative to its value for $\theta_{in} > 0$, at the same $\theta_{out}$, must be ascribed to the differences in absorption of the primary beam on the low- and high-angle sides. In fact, $f$ reaches its asymptotic value of unity only when both $\theta_{in}$ and $\theta_{out}$ are several hundred seconds away from the origin because of these primary extinction effects.

The very similar looking qualitative graph for the quantity corresponding to $f$ given by Afanas'ev *et al.* (1968) indicates that at these relatively large deviations from the Bragg angle the exact boundary conditions on the phonon-excited modes are not too important, because $\xi_{0H}(0) \gg \xi_{j0}(j)$.

Such variations in $f$ have also been discussed for X-rays in the symmetric two-beam Bragg geometry interacting with intense monochromatic phonons moving parallel to the surface (Juretschke & Wasserstein-Robbins, 1982).

Fig. 5 shows the value of $f/q_0$ resulting from (23) and (25) for the same two values of $\theta_{in}$ as used in Fig. 4. Since, apart from a constant factor, $f/q$ is proportional to the TDS of (24), it can be compared, on the one hand, with the corresponding kinematic result of Fig. 1 and, on the other, with the experimental data of EAP. Figs. 1 and 5 share a common overall scale, as well as the characteristic maximum on the side of the Bragg angle opposite to $\theta_{in}$. The maximum is shifted to a slightly smaller $\theta_{out}$ on the low-angle side relative to the prediction of (4), although this is unlikely to be discernible experimentally because the maximum is so broad. The same is probably true for the slight differences in the wings on opposite sides of $\theta_B$ introduced because $f$ reaches its asymptotic value so slowly from either above or below unity. The most important new features are carried over from the variation of $f$ near the Bragg angle in Fig. 4, producing a sharp peak and then a deep minimum in a low- to high-angle sweep, regardless of the sign of $\theta_{in}$. These features have no kinematical counterpart.

The comparison of Fig. 5 with the experimental results of EAP must take into account that various convolutions over the angular widths of the incident beam and over the detector acceptance angle may obscure some of the theoretically predicted details. Nevertheless, convolutions should not obscure the deep minimum around $\theta_{out} = 0$, which is independent of $\theta_{in}$. That it is not seen clearly in Figs. 2(*a*) and (*e*) of their paper must be ascribed to a lack of resolution of experimental points taken more than 5″ apart. The pronounced difference of their line shapes for $\theta_{in} = -65''$ and $\theta_{in} = 70''$ is not contained in the theory leading to Fig. 5, although the existence of the sharp peak on the low-angle side may give the appearance of some broadening for the positive relative to the negative $\theta_{in}$.

Since EAP's figures also show the elastically scattered peak at $\theta_{out} = \theta_{in}$, on the same scale, we can deduce an absolute magnitude of the observed inelastic scattering. At $\theta_{in} = -70''$, the elastic peak has a theoretical maximum of $1{\cdot}54 \times 10^{-3}$. From EAP's Fig. 2, therefore, the experimental inelastic peaks have a maximum close to $4 \times 10^{-4}$. After deconvoluting this intensity over an assumed 10″ width of the input beam, we expect that an inelastic peak intensity of $4 \times 10^{-5}('')^{-1}$ should be compared to the prediction of (24).

With representative values for the Ge 220 reflection and Cu $K\alpha$ radiation, the constant factor in (24) at $T = 300$ K is $3{\cdot}02 \times 10^{9}$ cm s$^{-2}('')^{-1}$. The value of $\langle g^2/v_p^2 \rangle$ depends on the orientation of the plane of incidence with respect to crystal axes. It can be shown to have an average value of $8{\cdot}25 \times 10^{-12}$ (cm s$^{-1}$)$^{-2}$, with a variation up to ±40% (Wasserstein-Robbins, 1982). With a typical value of $f/q_0 = 10^{-5}$ cm at the peak position, the prediction of (24) for the peak

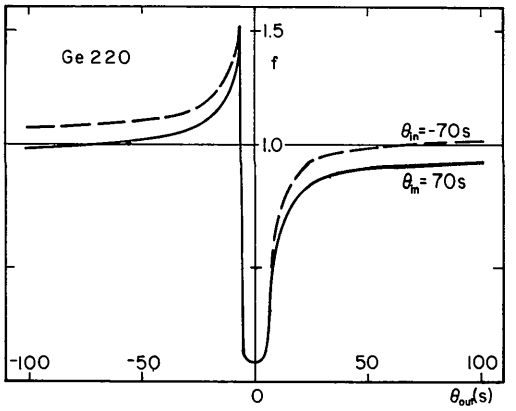


Fig. 4. Relative strength of dynamical X-ray phonon coupling $f$, defined by (23), *vs* $\theta_{out}$, for the Ge 220 reflection, at two offset angles $\theta_{in}$.

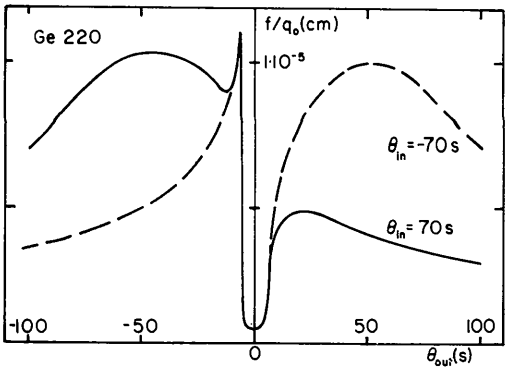


Fig. 5. Relative dynamical TDS structure $f/q_0$, based on (23) and (25), for the conditions of Fig. 4. This is the dynamical equivalent of Fig. 1.

TDS is $2{\cdot}5\times10^{-7}(")^{-1}$. This is more than two orders of magnitude below the peak seen by EAP. We therefore conclude that the observed peak is not caused by TDS, but must be due to other deviations from periodicity in the surface region of the crystal that have a similar Fourier spectrum as phonons. Since phonons are so slow, X-ray scattering at one temperature cannot distinguish between phonons and, for example, such static imperfections. A similar conclusion, based on corresponding experiments on Si, was reached by Iida & Kohra (1979). It should also be kept in mind that the position of the peak is relatively insensitive to the actual Fourier spectrum, and only requires that the diffusely scattered intensity increases as $q$ approaches its minimum cut-off for connecting two sheets of the dispersion surface at the given angle of incidence. For example, Afanas'ev *et al.* (1981) derive the same peak condition (4) for independently scattering small clusters of impurities in the surface region.

## 4. Discussion

Neither Eisenberger *et al.* (1972) nor Iida & Kohra (1979) were able to see the inelastic scattering features predicted by Fig. 5 near $\theta_{out}=0$. This is largely because the tails of their elastically scattered Bragg peak, centered at $\theta_{out}=\theta_{in}$, extend into the region near $\theta_{out}=0$ even though grooved crystals, with two and five reflections, respectively, were used in order to suppress these tails of the incident beam. Iida & Kohra (1979) ascribe the residual elastic peak seen at $\theta_{out}=0$ to inelastic scattering processes in the grooved-crystal surfaces, which keep the tail intensities of the beam incident on the sample substantially above theoretical expectations (Bonse & Hart, 1965). Until incident beams can be better defined, therefore, it will be difficult to substantiate the dynamical features of Fig. 5 in experiments that concentrate on very long phonons that require very small $\theta_{in}$.

However, one of the remarkable properties of the dip in intensity of Fig. 5 is that it always remains centered around $\theta_{out}=0$, regardless of the value of $\theta_{in}$. Hence, if $\theta_{in}$ is sufficiently large so that the incident beam produces no elastic scattering at $\theta_{out}=0$, the dip should be observable. Furthermore, because the dip is stationary, the angular resolution of the incident beam should not be an issue. Precisely this behavior has recently been reported (Kashiwase, Kainuma & Minoura, 1982) for incident X-ray beams more than 2° away from the Bragg angle. They ascribe the observed defect line normal to the plane of incidence to Bragg scattering of TDS. Wilkins, Chadderton & Smith (1983) concur in this general explanation, and embed it in the general formulation of the Kikuchi effects well known in electron diffraction. They also review earlier explanations of the observed defect lines, mostly seen in $\gamma$-ray scattering where elastic and inelastic processes are easily separated, and they explore the geometrical aspects of detecting the dips, as well as of using them in orienting crystals. Their conclusions are compatible with the dynamical theory presented here.

It should be mentioned, finally, that in both $\gamma$-ray and X-ray scattering such a defect line in the inelastic scattering is often also seen when $\theta_{in}\simeq 0$. Without question, this phenomenon has a similar dynamical origin to the effects treated here. However, in that case the theory of § 2 has to be modified, because several of its assumptions, such as the sharpness of the Lorentzian peak about the kinematic conservation of momentum, and the restriction to transitions involving either absorption or emission of a particular phonon, have to be re-examined. In addition, the observed signal is evidently a convolution over the angular width of the incident beam, and it is not obvious that in this region also the location and shape of the dip is independent of $\theta_{in}$. The extended theory for this case is the subject of the following paper (Juretschke, 1985).

We gratefully acknowledge correspondence with S. L. Schuster, and helpful discussions with N. G. Alexandropoulos.

### References


AFANAS'EV, A. M. & KAGAN, Y. (1967). *Acta Cryst.* **A24**, 163–170.

AFANAS'EV, A. M., KAGAN, Y. & CHUKOVSKII, F. N. (1968). *Phys. Status Solidi*, **28**, 287–294.

AFANAS'EV, A. M., KOVAL'CHUK, M. V., LOBANOVICH, E. F., IMAMOV, R. M., ALEKSANDROV, P. A. & MELKONYAN, M. K. (1981). *Sov. Phys. Crystallogr.* **26**, 13–17.

BATTERMAN, B. W. & COLE, H. (1964). *Rev. Mod. Phys.* **36**, 681–717.

BONSE, U. & HART, M. (1965). *Appl. Phys. Lett.* **7**, 238–240.

EISENBERGER, P., ALEXANDROPOULOS, N. G. & PLATZMAN, P. M. (1972). *Phys. Rev. Lett.* **28**, 1519–1522.

IIDA, A. & KOHRA, K. (1979). *Phys. Status Solidi A*, **51**, 533–542.

JAMES, R. W. (1965). *The Optical Principles of the Diffraction of X-rays*, ch. 5. Ithaca, NY: Cornell Univ. Press.

JURETSCHKE, H. J. (1985). *Acta Cryst.* **A41**, 598–603.

JURETSCHKE, H. J. & WASSERSTEIN-ROBBINS, F. (1982). *Phys. Rev. B*, **26**, 4262–4268.

KAINUMA, Y. (1961). *J. Phys. Soc. Jpn*, **16**, 228–241.

KASHIWASE, Y., KAINUMA, Y. & MINOURA, M. (1982). *Acta Cryst.* **A38**, 390–391.

KÖHLER, R., MÖHLING, W. & PEIBST, H. (1974). *Phys. Status Solidi B*, **61**, 173–180.

KURIYAMA, M. (1972). *Acta Cryst.* **A28**, 588–593.

O'CONNOR, D. A. (1967). *Proc. Phys. Soc.* **91**, 917–927.

SCHUSTER, S. L. (1969). PhD Thesis, Univ. of Nebraska.

SCHUSTER, S. L. & WEYMOUTH, J. W. (1971). *Phys. Rev. B*, **3**, 4143–4153.

WASSERSTEIN-ROBBINS, F. (1982). PhD Thesis, Polytechnic Institute of New York.

WASSERSTEIN-ROBBINS, F. & JURETSCHKE, H. J. (1983). *Bull. Am. Phys. Soc.* **28**, 47.

WILKINS, S. W., CHADDERTON, L. T. & SMITH, T. F. (1983). *Acta Cryst.* **A39**, 792–800.

WILLIS, B. T. M. & PRYOR, A. W. (1975). *Thermal Vibrations in Crystallography*, ch. 7. Cambridge Univ. Press.